ORIGINAL ARTICLE

Cancer Science WILEY

Overcoming immunotherapy resistance and inducing abscopal effects with boron neutron immunotherapy (B-NIT)

Takuya Fujimoto[1,2] | Osamu Yamasaki[3,4] | Noriyuki Kanehira[1,2] | Hirokazu Matsushita[5] |
Yoshinori Sakurai[6] | Naoya Kenmotsu[7,8] | Ryo Mizuta[5,8] | Natsuko Kondo[6] |
Takushi Takata[6] | Mizuki Kitamatsu[9] | Kazuyo Igawa[2] | Atsushi Fujimura[2,10] |
Yoshihiro Otani[8] | Makoto Shirakawa[2] | Kunitoshi Shigeyasu[1] | Fuminori Teraishi[1] |
Yosuke Togashi[7] | Minoru Suzuki[6] | Toshiyoshi Fujiwara[1] | Hiroyuki Michiue[2]

[1]Department of Gastroenterological Surgery, Okayama University Graduate School of Medicine, Dentistry, and Pharmaceutical Sciences, Okayama, Japan

[2]Neutron Therapy Research Center, Okayama University, Okayama, Japan

[3]Department of Dermatology, Okayama University Graduate School of Medicine, Dentistry, and Pharmaceutical Sciences, Okayama, Japan

[4]Department of Dermatology, Shimane University Faculty of Medicine, Izumo, Japan

[5]Division of Translational Oncoimmunology, Aichi Cancer Center Research Institute, Nagoya, Japan

[6]Institute for Integrated Radiation and Nuclear Science, Kyoto University, Sennan-gun, Japan

[7]Department of Tumor Microenvironment, Okayama University Graduate School of Medicine, Dentistry, and Pharmaceutical Sciences, Okayama, Japan

[8]Department of Neurological Surgery, Okayama University Graduate School of Medicine, Dentistry, and Pharmaceutical Sciences, Okayama, Japan

[9]Faculty of Science and Engineering, Kindai University, Higashiosaka, Japan

[10]Department of Physiology, Okayama University Graduate School of Medicine, Dentistry, and Pharmaceutical Sciences, Okayama, Japan

Correspondence
Hiroyuki Michiue, Neutron Therapy Research Center, Okayama University, 2-5-1 Shikata-cho, Kita-ku, Okayama 700-8558, Japan.
Email: hmichiue@md.okayama-u.ac.jp

Abstract

Immune checkpoint inhibitors (ICIs) are effective against many advanced malignancies. However, many patients are nonresponders to immunotherapy, and overcoming this resistance to treatment is important. Boron neutron capture therapy (BNCT) is a local chemoradiation therapy with the combination of boron drugs that accumulate selectively in cancer and the neutron irradiation of the cancer site. Here, we report the first boron neutron immunotherapy (B-NIT), combining BNCT and ICI immunotherapy, which was performed on a radioresistant and immunotherapy-resistant advanced-stage B16F10 melanoma mouse model. The BNCT group showed localized tumor suppression, but the anti-PD-1 antibody immunotherapy group did not show tumor suppression. Only the B-NIT group showed strong tumor growth inhibition at both BNCT-treated and shielded distant sites. Intratumoral CD8+ T-cell infiltration and serum high mobility group box 1 (HMGB1) levels were higher in the B-NIT group. Analysis of CD8$^+$ T cells in tumor-infiltrating lymphocytes (TILs) showed that CD62L- CD44$^+$ effector memory T cells and CD69$^+$ early-activated T cells were predominantly increased in the B-NIT group. Administration of CD8-depleting mAb to the B-NIT group completely suppressed the augmented therapeutic effects. This

indicated that B-NIT has a potent immune-induced abscopal effect, directly destroying tumors with BNCT, inducing antigen-spreading effects, and protecting normal tissue. B-NIT, immunotherapy combined with BNCT, is the first treatment to overcome immunotherapy resistance in malignant melanoma. In the future, as its therapeutic efficacy is demonstrated not only in melanoma but also in other immunotherapy-resistant malignancies, B-NIT can become a new treatment candidate for advanced-stage cancers.

1 | INTRODUCTION

Programmed cell death-1 (PD-1) was discovered by Ishida and Honjo et al. in 1992 as a molecule that induces T-cell death.[1] These discoveries ushered in a new era of cancer immunotherapy, a strategy that induces tumor suppression by targeting the immune evasion mechanisms of cancer cells, and led to the development of anti-PD-1 antibodies as immune checkpoint inhibitors (ICIs).[2–4] The success of ICI-based immunotherapy for advanced melanoma resulted in the application of ICI for many advanced malignancies in clinical practice.[4,5] In the CheckMate 067 phase III trial of dual ICI nivolumab (an anti-PD-1 antibody) and ipilimumab (an anti-CTLA-4 antibody) for advanced malignant melanoma, the 5-year survival rate for dual ICI immunotherapy was 52% compared with 40% for nivolumab alone and 20% for ipilimumab alone.[6] However, while dual ICI immunotherapy with antibodies targeting CTLA-4 and PD-1 was very effective, the frequency of treatment-related adverse events was high, and 139 of 313 patients in the dual ICI immunotherapy group discontinued treatment.[6–8] A phase II study (ONO-4358) of nivolumab alone in advanced malignant melanoma in Japan showed a 5-year survival rate of 26.1%, which was lower than the results in CheckMate 067.[9] The most common types of malignant melanoma in Japan and Asia are acral lentiginous (29.2%) and mucosal (25.0%), while these types are less common in Caucasians (3.0% and 6.9%, respectively). The 5-year survival rate for the superficial extension type, which is more common in Caucasians, was as high as 66.7%, while the rates for the acral lentiginous and mucosal types were 14.3% and 16.7%, respectively, indicating that the prognosis of nivolumab monotherapy varies depending on the type of melanoma.[9] Therefore, combination therapy with immunotherapy should be further explored to improve the prognosis of many immunotherapy-resistant patients.

Boron neutron capture therapy (BNCT) uses a system consisting of two components (boron and neutrons) to produce a therapeutic effect against tumors.[10] The boron isotope ^{10}B (3990 burns) is extremely rare in living tissue but is highly reactive with neutrons.[10] Furthermore, the range of particles produced by the alpha decay with boron and neutrons is very short, and the reactive range is at the cellular level. Clinical studies of BNCT were initiated in 1951, but the results of studies conducted over the subsequent 10 years were not satisfactory.[11] The reasons were that the neutron field was not safe and that no boron drugs were able to concentrate at high amounts in cancer cells. In 1987, Mishima et al. achieved excellent results in a clinical trial for BNCT for malignant melanoma using 4-borono-L-phenylalanine (BPA) as a drug that exhibited melanoma-specific uptake. BPA was initially created as a phenylalanine-fused boron drug for BNCT specific for melanoma, which has high melanin biosynthesis in vivo.[12] BPA was found to be taken up not only by melanoma cells but also by cells of various malignancies with high amino acid metabolism, leading to successful treatment with BPA-BNCT.[13] After multiple basic and clinical studies at the Kyoto University Research Reactor Institute and other institutions, an accelerator neutron source that could be installed in a hospital was successfully developed, and in 2020, the world's first insurance-approved clinical BNCT treatment for unresectable locally advanced or locally recurrent head and neck cancer was launched in Japan.[14–17]

In this study, the results showed that BNCT combination therapy overcomes the nonresponse to ICI immunotherapy.

2 | MATERIALS AND METHODS

2.1 | Cell line and cell culture

The mouse melanoma cell line B16F10 (TKG0348) was obtained from the Cell Resource Center, Tohoku University (Japan) and cultured B16F10 cells were cultured in their protocol.

2.2 | Advanced melanoma mouse model

All animal use and care procedures were conducted by ARRIVE 2.0 guidelines. C57BL/6J mice (female, 6–8 weeks, 16–20 g, Japan CLEA, Inc.) were reared in plastic cages (Clare Japan Inc.) using a positive pressure unidirectional airflow rearing rack (AP Anicon, Seiken Corporation) under the following conditions: temperature 20–25°C, humidity 40%–60%, ventilation in the cage at least 50 times/h, light/dark cycle 12/12 h, and lighting at 8:00 AM. To establish the

advanced melanoma model, mice were subjected to right hind leg intradermal injection of B16F10 cells (3×10^5 cells per mouse) and left flank subcutaneous injection of B16F10 cells (5×10^5 cells per mouse) (Approved# OKU-2021447).

2.3 | Inductively coupled plasma (ICP) measurement of boron

One week after cell implantation, BPA at 500 mg/kg (Stella Pharma Corporation) was intraperitoneally or subcutaneously administered. The mice were euthanized 0.5, 1, 2, 3, 6, or 12 h after BPA administration, and tumors and organs were collected under general anesthesia ($n = 4$ mice/group). The samples were soaked in 70% nitric acid at 90°C for 1 h. After filtering the samples with a syringe filter (0.5 μm), the amount of boron in the samples was quantified using ICP-MS (Agilent 7900 ICP-MS) at Okayama University Institute of Plant Science and Resources.

2.4 | Mouse treatment methods

Mouse anti-PD-1 (250 μg per mouse, Bio X Cell, # BE0146) was intraperitoneally administered on day 4 or 7. On the following day, mice were anesthetized (medetomidine 0.3 mg/kg + midazolam 4 mg/kg + betorphanol 5 mg/kg), and 500 mg/kg BPA was subcutaneously injected. After 1 h, 5 MW neutron irradiation was performed for 12 min. At day 10 and 13, mouse anti-PD1 (250 μg per mouse) was intraperitoneally administered. For depletion of CD8$^+$ T cells, InVivoMAb anti-mouse CD8 mAb (200 μg per mouse, Bio X Cell, # BE0117) was intraperitoneally administered on day 3, 5, 9, and 13.

2.5 | Dose estimation for BNCT

The total BNCT dose consists of a nitrogen dose, hydrogen dose, gamma ray dose, and boron dose.

2.6 | ELISA

Blood was collected with a heparin-treated syringe. Serum HMGB1 was measured with a commercial ELISA kit following the manufacturer's protocol (ARG81310, Arigo Biolaboratories).

2.7 | Immunohistochemistry

Tumor tissues were collected from mice and fixed with 4% paraformaldehyde for 4 h, followed by cryoprotection in 30% sucrose for 1 day at 4°C. The frozen section was incubated with mouse anti-CD8a (eBioscience, 4SM15), followed by incubation with rat IgG-conjugated Alexa-Fluor 594 for 2 h, Hoechst 33258 for 30 min. Immunohistochemistry was observed with an all-in-one fluorescence microscope (BZ-X800, KEYENCE).

2.8 | LAT1 gene expression analysis

The cBioPortal for Cancer Genomics (http://cbioportal.org) and The Cancer Genome Atlas (TCGA, https://www.cancer.gov/tcga) were used to explore, visualize, and analyze multidimensional cancer genomics data of LAT1 expression.

2.9 | Cell preparation and flow cytometry

Mouse disaggregated cells prepared from mouse tissue or tumor were first stained with the Zombie Aqua™ Fixable Viability Kit (BioLegend) to label dead cells, pretreated with Fc Block, and incubated with fluorescence-labeled antibodies. The stained cells were washed and then analyzed with an LSRFortessa™ X-20 (BD Biosciences) and FlowJo Software (BD Biosciences). The detailed method is shown in Figure S1.

2.10 | Neutron irradiation experiments in KURNS

Model mice were fixed in a mouse holder under trichloroanesthesia (medetomidine 0.3 mg/kg, midazolam 4 mg/kg, butorphanol 5 mg/ kg). Twelve mice were fixed circumferentially and irradiated in I Kyoto University Institute for Integrated Radiation and Nuclear Science (KURNS) (approved# KURNS-2021-39). Details are described in Figures S2–S5.

2.11 | Statistical analysis

Statistical analysis was conducted using Student's t-test, one-way analysis of variance (ANOVA), two-way ANOVA, and nonparametric statistics (Mann–Whitney U test) with post hoc analysis. p-Values less than 0.05 were considered statistically significant. All data were analyzed using Microsoft Excel 2019 of Microsoft Office Professional Plus 2019 and GraphPad Prism version 7.

3 | RESULTS

3.1 | Pharmacokinetics of BPA

BPA is a tumor-selective BNCT boron agent with reported high uptake in melanoma with high melanin biosynthesis (Figure 1A) and many malignancies with high amino acid transporter LAT-1 expression, particularly head and neck cancer and malignant brain tumors (Figure 1B).

(A)

(B)

(C)

C57BL/6J
B16-F10 murine melanoma
🔴 Rt. Intramuscular cell implantation
🔵 Lt. Subcutaneous cell implantation

(D)

Subcutaneous administration (BPA 500mg/kg)

(E)

Intraperitoneal administration (BPA 500mg/kg)

(F)

Subcutaneous administration
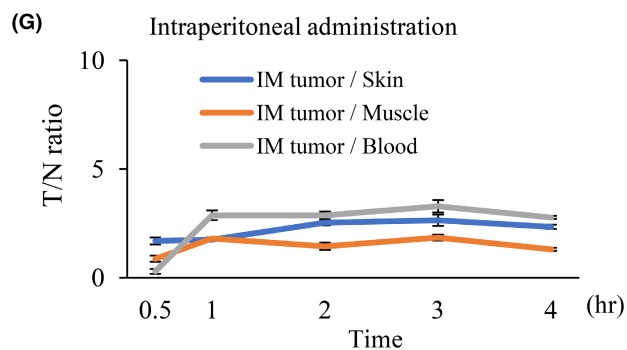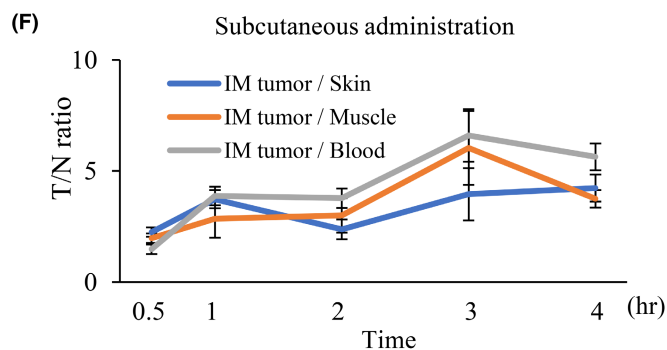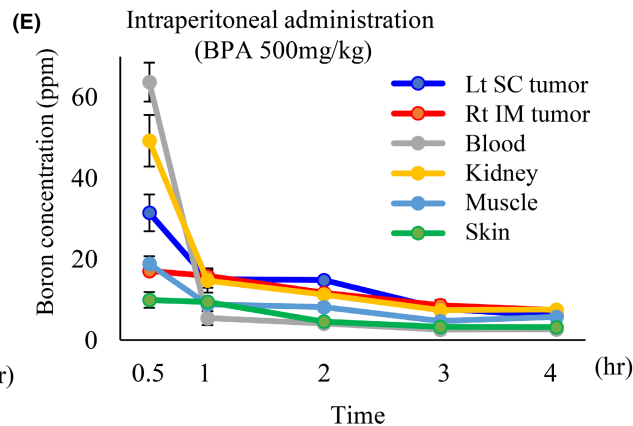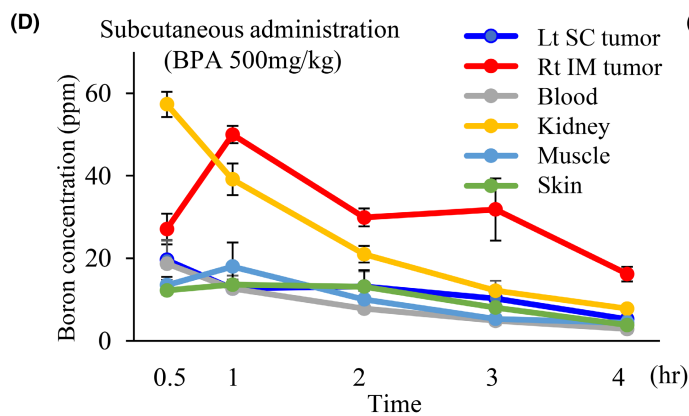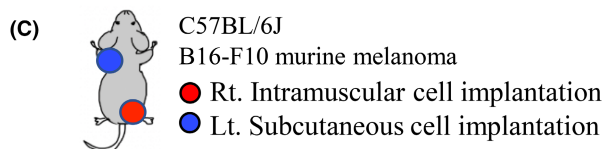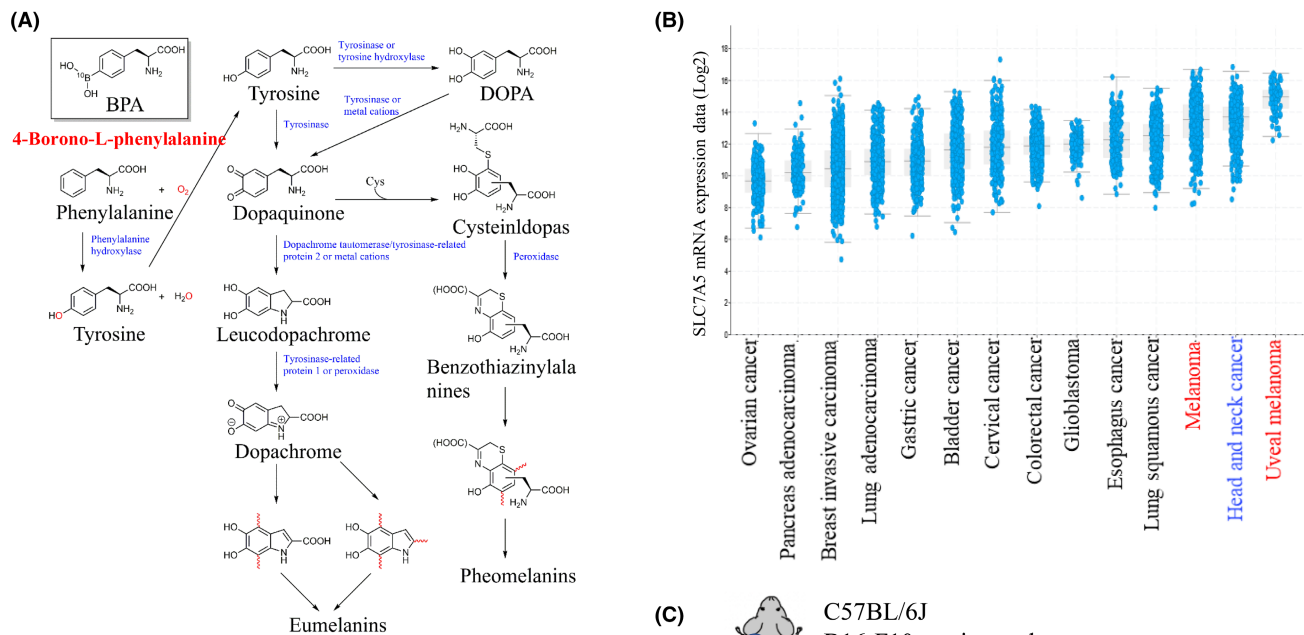
Time from adm. (hr)		0.5	1	2	3	4
TN ratio	IM tumor / skin	2.2	3.7	2.3	4.0	4.2
	IM tumor / muscle	2.0	2.8	3.0	6.0	3.7
TB	IM tumor / blood	1.4	3.9	3.8	6.6	5.6

(G)

Intraperitoneal administration

Time from adm. (hr)		0.5	1	2	3	4
TN ratio	IM tumor / skin	1.7	1.7	2.5	2.6	2.3
	IM tumor / muscle	0.9	1.8	1.4	1.8	1.3
TB	IM tumor / blood	0.3	2.9	2.9	3.3	2.8

FIGURE 1 Pharmacokinetics of 4-borono-L-phenylalanine (BPA) in an advanced-stage melanoma model. (A) BPA is a phenylalanine-bound boron drug and a melanoma-targeted boron neutron capture therapy (BNCT) drug with high melanoma biosynthesis.(B) Comparison of mRNA SLC7A5 (LAT1) with TCGA. (C) Mouse model of advanced-stage melanoma with C57BL/6J/ and B16F10 cells transplanted intramuscularly in the right thigh and subcutaneously in the left flank. (D, E) Boron concentration pharmacokinetics in a mouse model of advanced-stage melanoma (subcutaneous [D] or intraperitoneal administration [E], BPA 500mg/kg, $n=4$ at each time point). (F, G) Tumor-to-normal tissue (T/N) ratio: Ratio of boron concentration in right thigh intramuscular tumor and normal tissue (muscle, skin, blood) administered subcutaneously (F) or intraperitoneally (G).
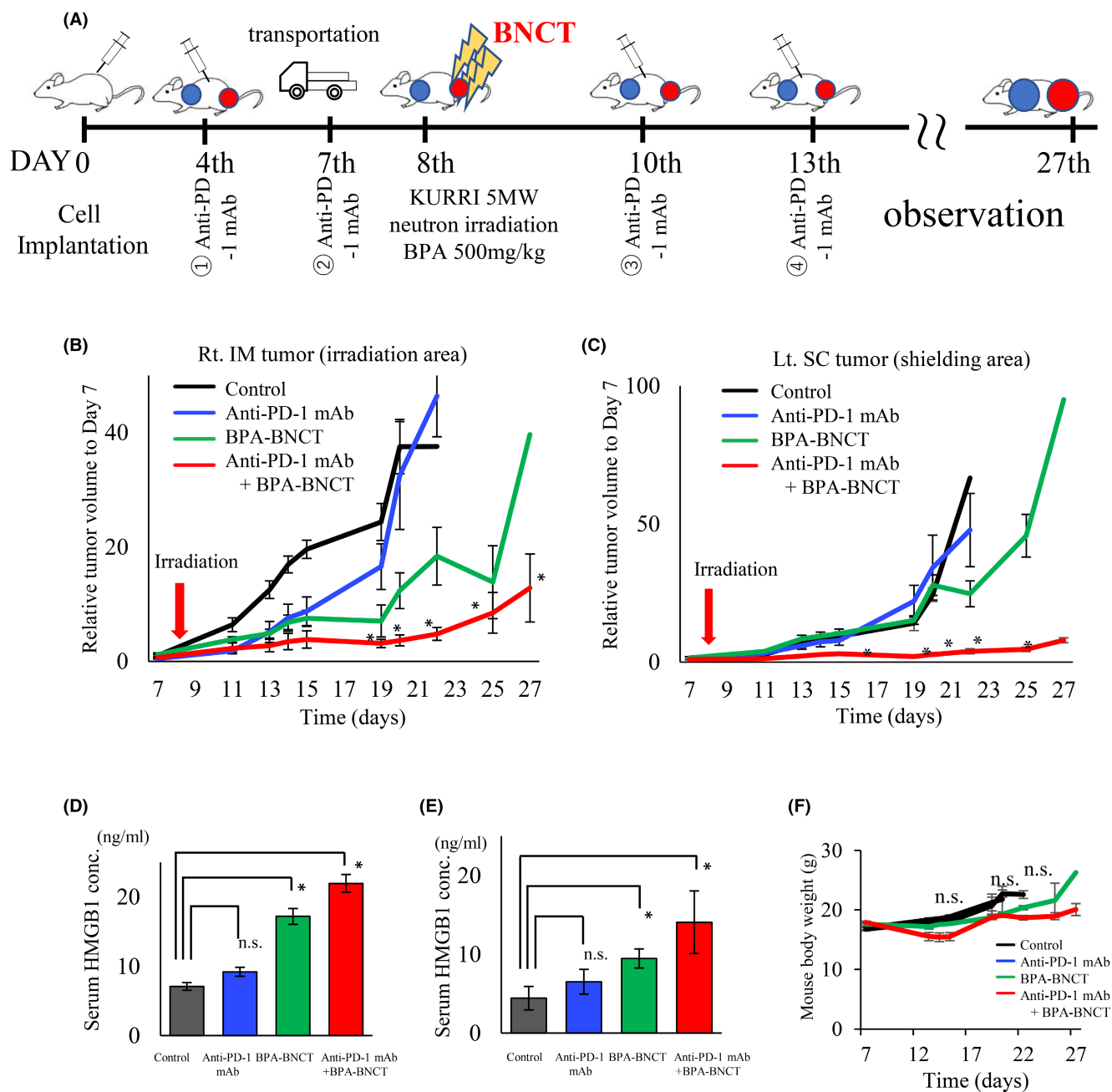
FIGURE 2 The antitumor results of boron neutron immunotherapy (B-NIT) in the advanced-stage melanoma model. (A) Schematic of the time course of the B-NIT experiments. (B, C) Tumor volume of the right thigh intramuscular tumors at the neutron irradiation site (B) and the left abdominal subcutaneous tumor at the shielded site (C) in the four groups. The tumor volume ratio was determined to tumor volume at day 7 after cell transplantation. *$p<0.05$. (D, E) Serum HMGB1 concentration (ng/mL) on day 15 (D) and the final stage (E) after neutron irradiation. *$p<0.05$. (F) Mouse body weight changes in the four groups over time ($n=6$/group). BNCT, boron neutron capture therapy.

The LAT1 protein is one of the system L amino acid transporters that transport essential amino acids such as phenylalanine with high affinity and a target protein of the boron drug BPA. We compared the expression of SLC7A5 (solute carrier family 7 member 5, which encodes LAT1) across many cancer types using TCGA (Figure 1B). The expression of SLC7A5 was higher in melanoma compared with other cancers.

Pharmacokinetic (PK) evaluation of BPA was performed in a mouse model of advanced-stage melanoma. To establish the model, B16F10 melanoma cells were transplanted intramuscularly in the right thigh and subcutaneously in the left flank. BPA (500 mg/kg) was then administered intraperitoneally or subcutaneously (Figures 1C–G). Subcutaneous administration of BPA resulted in approximately 50 ppm ^{10}B in the right intramuscular (IM) tumor and 12.7 ppm ^{10}B in the left subctaneous (SC) tumor after 1 h (Figures 1D,F); the tumor-to-normal tissue boron concentration ratio (T/N ratio) was T/N (skin) ratio = 3.7, T/N (muscle) ratio = 2.8, and T/N (blood) ratio = 3.9 (Figures 1D,F). In the intraperitoneal group, approximately 30 ppm ^{10}B was found in the right tumor and 15.1 ppm ^{10}B in the left tumor, with T/N ratios of T/N (skin) ratio = 1.7, T/N (muscle) ratio = 1.8 and T/N (blood) ratio = 2.9 (Figures 1E,G). Hence, we selected subcutaneous administration of BPA because of the high boron concentration in the right lower extremity intramuscular tumor at the irradiation site and the low boron concentration in the left abdominal subcutaneous tumor within the shielding site.

3.2 | Boron neutron immunotherapy (B-NIT) treatment strategy for advanced melanoma model mice

Next, BNCT with immunotherapy was administered to mice modeling advanced-stage melanoma (Figure 2A). The mouse melanoma model of B16F10 transplantation into C57BL/6 is being used as a model of resistance to ICI in many papers.[18,19]

At the neutron-irradiated site, tumor volume ratios on day 22 were 37.6 (control group), 46.4 (anti-PD-1 mAb group), 18.4 (BNCT group), and 3.7 (B-NIT group) (Figure 2B). On the other hand, the tumor volume ratio of the shielded remote site was 66.6 (control group), 47.8 (anti-PD-1 mAb group), 24.7 (BNCT group), and 3.9 (B-NIT group), and the immune effect was confirmed (Figure 2C).

As for blood high mobility group box 1 (HMGB1), a representative marker of damage-associated molecular patterns (DAMPs), serum HMGB1 levels on day 12 were similar in the control (7.08 ng/mL) and anti-PD-1 mAb groups (9.20 ng/mL, $p = 0.0514$), but not in the BPA-BNCT group (17.19 ng/mL, $p < 0.001$) and B-NIT group (21.95 ng/mL, $p < 0.001$). (Figure 2D). HMGB1 levels at the final stage of analysis (days 22–27) remained elevated in the control (3.46 ng/mL) and anti-PD-1 mAb groups (4.26 ng/mL, $p = 0.1046$) and in the BPA-BNCT (9.46 ng/mL, $p < 0.001$) and B-NIT (14.07 ng/mL, $p < 0.001$) were (Figure 2E). There was no significant difference in body weight among the four groups during the observation period (Figure 2F).

3.3 | Principle of BNCT, dose calculation, and neutron irradiation system

Boron–neutron capture therapy is a therapy that utilizes alpha-decay, a reaction between boron isotope ^{10}B and neutrons[20] (Figure 3A). A neutron irradiation system was constructed using lithium fluoride (LiF) for neutron shielding (Figure 3B). Recently, the neutron source has been changed from a reactor neutron source to an accelerator neutron source that can be installed in hospitals. The treatment dose for BNCT is described in detail in Figure 3C. Right hind leg intramuscular tumors were included in the irradiation field, and left flank subcutaneous tumors were at the shielding sites (Figures 3B,D–F). Calculation of the radiological dose was 37.3 Gy-Eq (right tumor), 6.9 Gy-Eq (muscle), and 9.9 Gy-Eq, (skin) (Figure 3E and Figures S2–S5). The thermal neutron dose ratio to the irradiated and the nonirradiated areas was 6.5:1 (Figure 3D). The thermal neutron intensities at the proximal and distal parts of the neutron source were 2.8×10^{12} and 2.2×10^{12} (n·cm^{-2}), respectively, and the ratio was 0.8 (Figure 3D). For the right proximal IM tumor, right distal IM tumor, and left SC tumor, the boron doses were 39.49, 30.28, and 1.39, the nitrogen doses were 1.14, 0.87, and 0.16 (Gy-Eq), the hydrogen doses were 1.01, 0.77, and 014 (Gy-Eq), and the gamma ray doses were 0.52, 0.56, and 0.33, respectively (Figure 3E, and Figures S2–S5).

3.4 | Therapeutic effects of B-NIT

In the tumor tissue of the right thigh (irradiation site), a high density of CD8$^+$ T cells was identified in the BNCT and B-NIT on day 22 (Figure 4A). In the left tumor (shielded site), CD8$^+$ T cells were

FIGURE 3 Overview of therapeutic radiation dose of boron neutron immunotherapy (B-NIT) for the advanced-stage mouse melanoma model. (A) Production of high-energy ^7Li and ^4He by alpha decay between boron-10 nuclides and neutrons (top) and a schematic diagram of boron neutron capture therapy (BNCT) for cancer therapy (bottom). (B) Experimental diagram of the neutron irradiation/shielding system and neutron/gamma ray biomarker during irradiation of the mice. (C) The total biological dose for BNCT consists of the nitrogen dose, hydrogen dose, gamma ray dose, and boron dose. (D) Average thermal neutron fluence at each mouse site after 5 MW, 12 min neutron irradiation at KURRI (n/cm^2, each $n = 6$). (E) Mean total irradiation dose results for each tissue after BNCT (Gy-Eq, each $n = 6$). (F) Boron dose results, nitrogen dose results, hydrogen dose results, and gamma radiation dose results (Gy-Eq, each $n = 6$) at three sites (left flank subcutaneous tumor site, right lower limb proximal, and distal intramuscular tumor) by neutron irradiation. (D–F) Red bars indicate results for neutron-irradiated areas; blue shaded bars indicate results for shielded areas.

(A)

$$^{10}B + {}^{1}n \rightarrow {}^{7}Li + \alpha(^{4}He)$$

Neutron

Cancer cell

Normal cells

$\alpha(^4He)$

^{10}B

$9\mu m$

$4\mu m$

^7Li

nucleus

Neutron

$15\text{-}20\mu m$

Cancer cells

(B)

LiF   LiF

Neutron shielding

Neutron Source

LiF

Neutron

Lt SQ tumor

LiF

Au

Au

Neutron

Rt distal IM tumor

Rt proximal IM tumor

Neutron

(C)

Biological Dose for BNCT

Components	RBE or CBE-weighted dose (Gy-Eq)
Nitrogen dose	$E_N = RBE_N \times D_N$
Hydrogen dose	$E_H = RBE_H \times D_H$
Gamma ray dose	$E_\gamma = RBE_\gamma \times D_\gamma$
Boron dose	$E_B = C_{B10} \times CBE \times D_{B10=1ppm}$
Total dose	$E_{total} = E_{thermal} + E_{epi} + E_{fast} + E_\gamma + E_B$

D_N : absorbed dose for N-14(n,p)C-14 reaction (Gy-Eq)
D_H : absorbed dose for H-1(n,n)H-1 reaction (Gy-Eq)
$D_{B10=1ppm}$: absorbed dose for B-10(n,α)Li-7 reaction
       for B-10 concentration of 1 ppm (Gy-Eq)
RBE : relative biological effectiveness
CBE : compound biological effectiveness
C_{B10} : concentration of B-10 in tissue (ppm)
       Here, RBE_N=3, RBE_H=3, RBE_γ=1

Dose advantage over normal tissue

Total tumor dose of BNCT

E_B

E_B

E_γ

E_γ

E_H

E_H

E_N

E_N

Non-boron dose

Tumor tissue

Normal tissue

(D)

Thermal neutron (~0.5eV)

Irradiation area

Shielding area

Thermal neutron fluence (n/cm2)

3.00E+12

2.00E+12

1.00E+12

0.00E+00

Lt SQ tumor | Rt distal IM tumor | Rt proximal IM tumor

(E)

Total irradiation dose (Gy-Eq)

40

30

20

10

0

Irradiation area

Shielding area

Rt. IM tumor | Normal muscle | Lt. SC tumor | Normal skin

	Rt. IM tumor	Normal muscle	Lt. SC tumor	Normal skin
CBE	3.8	1.35	3.8	2.5
10B conc. (ppm)	50	18	13	14

(F)

Boron dose

Irradiation area

Shielding area

Irradiation dose (Gy-Eq)

40

30

20

10

Lt SQ tumor | Rt distal IM tumor | Rt proximal IM tumor

Nitrogen dose

Irradiation area

Shielding area

Irradiation dose (Gy-Eq)

1.5

1

0.5

0

Lt SQ tumor | Rt distal IM tumor | Rt proximal IM tumor

Hydrogen dose

Irradiation area

Shielding area

Irradiation dose (Gy-Eq)

1.2

0.8

0.4

0

Lt SQ tumor | Rt distal IM tumor | Rt proximal IM tumor

Gamma ray dose

Irradiation area

Shielding area

Irradiation dose (Gy-Eq)

0.6

0.4

0.2

0

Lt SQ tumor | Rt distal IM tumor | Rt proximal IM tumor

accumulated only in the B-NIT (Figure 4B). Flow cytometry analysis of TILs in the right intramuscular tumors on day 12 revealed high levels of TILs in the BPA-BNCT and B-NIT groups (control: 24.6%, anti-PD-1 mAb: 25.3%, BPA-BNCT: 49.2%, B-NIT: 64.6%, Figure 4C). Analysis of TILs in the left subcutaneous tumors showed high levels of CD8+ T cells in the B-NIT group compared with other groups (control: 14.4%, anti-PD-1 mAb: 14.1%, BPA-BNCT: 12.1%, B-NIT: 45.6%, Figure 4D). Immunostaining also showed strong intratumor localization of CD8+ cells in the B-NIT group (Figure 4B). An increase in splenic CD8+ T cells was observed in both the BPA-BNCT and B-NIT groups compared with the control, and the increase was more pronounced in the B-NIT (control: 5.4%, anti-PD-1 mAb: 7.2%, BPA-BNCT: 10.2%, B-NIT: 14.4%, Figure 4E). Representative flow cytometry data of TILs in each tissue are shown in Figure 4F.

3.5 | CD8+ effector memory T cells (TEMs) of TILs with B-NIT

First, we focused on memory T cells, an important component of the tumor-adaptive immune system, and its subset of CD8+ TEMs. Evaluation of CD44+ CD62L− TEMs revealed a high tumor immunological effect induced by B-NIT in the right tumor area at the irradiation site (Figures 5A,B, $p < 0.0001$) and left tumor area at the shielding site (Figures 5C,D, $p < 0.0001$). There were increased levels of TEMs at the irradiation site in the B-NIT (66.1%) compared with the control (24.5%) (Figures 5B,E). There were also more TEMs at the shielded site in the B-NIT compared with the control (control: 43.0%, B-NIT: 82.7%) (Figure 5F). In all cases, the percentage of TEMs was predominantly increased in the B-NIT compared with the control ($p < 0.0001$) (Figure 5G).

3.6 | Early-activated T cells of TILs

Flow cytometry data showed early-activated T cells (CD8+ CD69+) in the BNCT-treated area and the shielded distant sites (Figures 6A,B). In the right intramuscular tumor area, the percentage of early-activating T cells was 59.9% in the control and 66.6% in the B-NIT, with no significant difference (Figure 6A, $p = 0.0523$). In the left subcutaneous tumor area, the percentage of early-activating T cells was 41.6% in the control and 64.6% in the B-NIT, with a significant difference between the two (Figure 6B, $p < 0.0001$). In the comparison of the four groups, early-activating T cells were predominantly elevated only in the shielded area in the B-NIT (Figure 6C).

The results from the TIL analysis showed that TEMs were predominantly elevated at both BNCT-treated and distant sites; for early-activating T cells, the elevation was predominant only at distant sites.

3.7 | The antitumor effect of B-NIT without neutron irradiation

We next performed a COLD experiment without neutron irradiation using the same model (Figures 7A,B). There was no tumor volume difference among the four groups. There were also no differences in CD45+ CD8+ T cells in the spleen (Figure 7C), body weight (Figure 7D), or serum HMGB1 levels (Figure 7E). Thus, no tumor-suppressive effect, including the abscopal effect, was observed in the COLD experiment.

3.8 | The CD8+ cellular immune effects of B-NIT

To confirm that the immunotherapeutic effect of CTL was an antitumor effect of CD8+ T cells, anti-CD8+ mAb was administered (Figure 8A). Both BNCT and B-NIT showed marked tumor suppression in tumors at the BNCT direct treatment site with anti-CD8+ mAb administration (Figure 8B, $p < 0.01$). However, the abscopal effect was suppressed by anti-CD8+ mAb administration (Figures 8C–E). The treatment tumor doses were 27.1 Gy in right and 1.8 Gy in left (Figure S6). Flow cytometry results of representative cases showed that the CD45+ CD8+ cells were almost 0% in tumors and spleen in all (Figure 8G and Figure S7). Serum HMGB1 was markedly elevated in the BNCT. But B-NIT with CD8+ antibody did not show any effect on tumor shrinkage (Figure 8G). There were no significant differences in body weight among the four groups (Figure 8H).

4 | DISCUSSION

This is the first paper to demonstrate the abscopal effect induced by the combination of BNCT and ICI in an ICI-resistant melanoma model. In a preclinical mouse model of advanced ICI-resistant B16F10 melanoma, direct tumor destruction by BNCT with protection of normal tissue induced a distal bystander effect by activating cellular immune activity by CD8+ T cells under anti-PD-1 antibody treatment through the spread of tumor antigen and sustained release of DAMPs (Figure 9A). Next, B-NIT is expected to show therapeutic efficacy in clinical trials in advanced-stage melanoma

---

FIGURE 4 Results in four groups of CD8+ immune cells in tumor and spleen. (A, B) Immunohistochemistry image of CD8+ (red) and nuclear staining (blue) of right thigh intramuscular tumors (A) and left flank subcutaneous tumors (B) on day 22 in the four groups (scale bars, 100 μm). (C–E) Flow cytometry analysis of CD8+ T cells in CD45+ cells in right-thigh intramuscular tumors (C), left-abdominal subcutaneous tumors (D), and spleen (F) on day 15 (*$p < 0.05$). (F) Representative flow cytometry results of CD8+ T cells with CD45+ cells in control group, anti-PD-1 group, BPA-BNCT group and B-NIT group. B-NIT, boron neutron immunotherapy; BNCT, boron neutron capture therapy; BPA, 4-borono-L-phenylalanine.
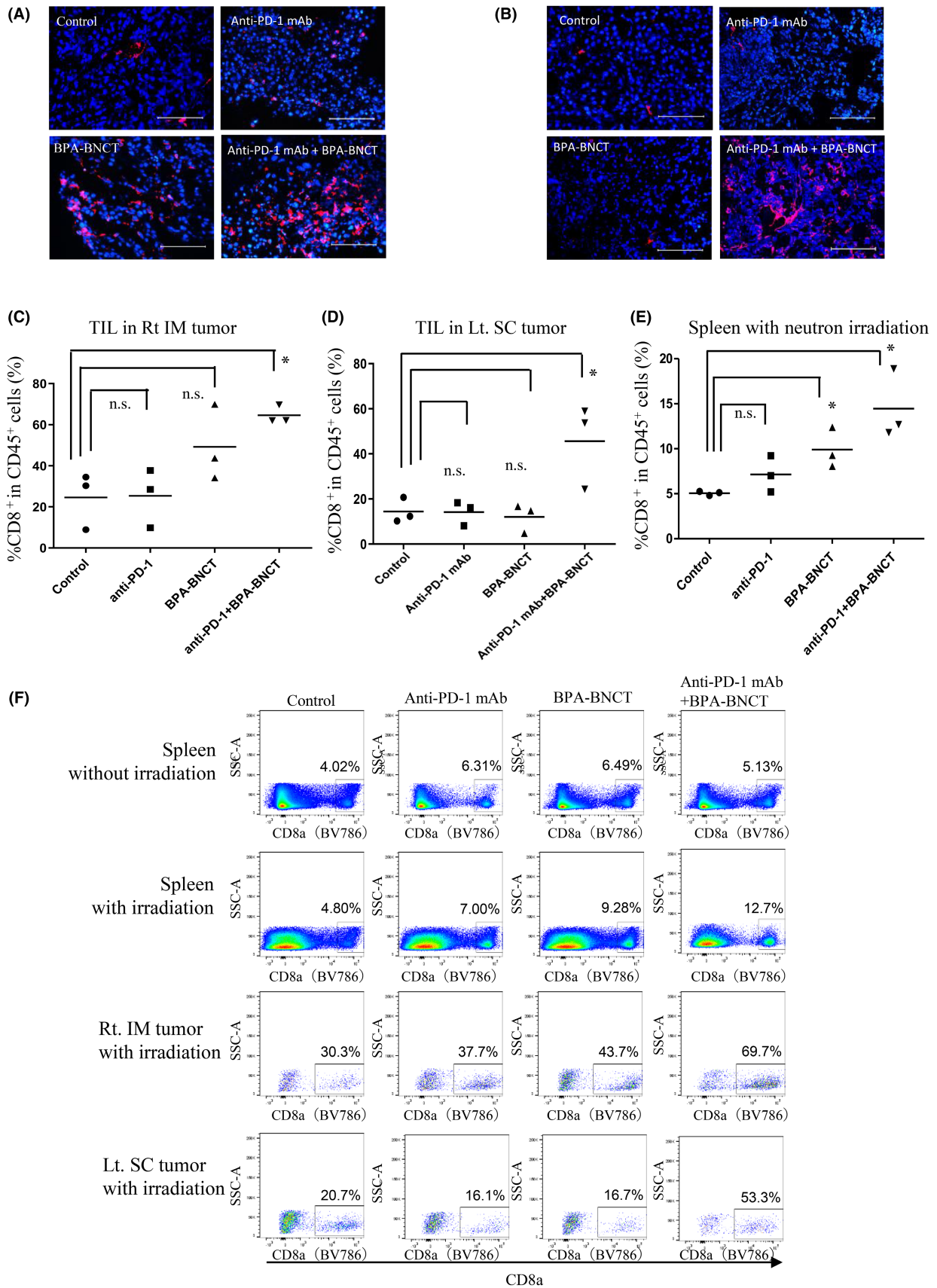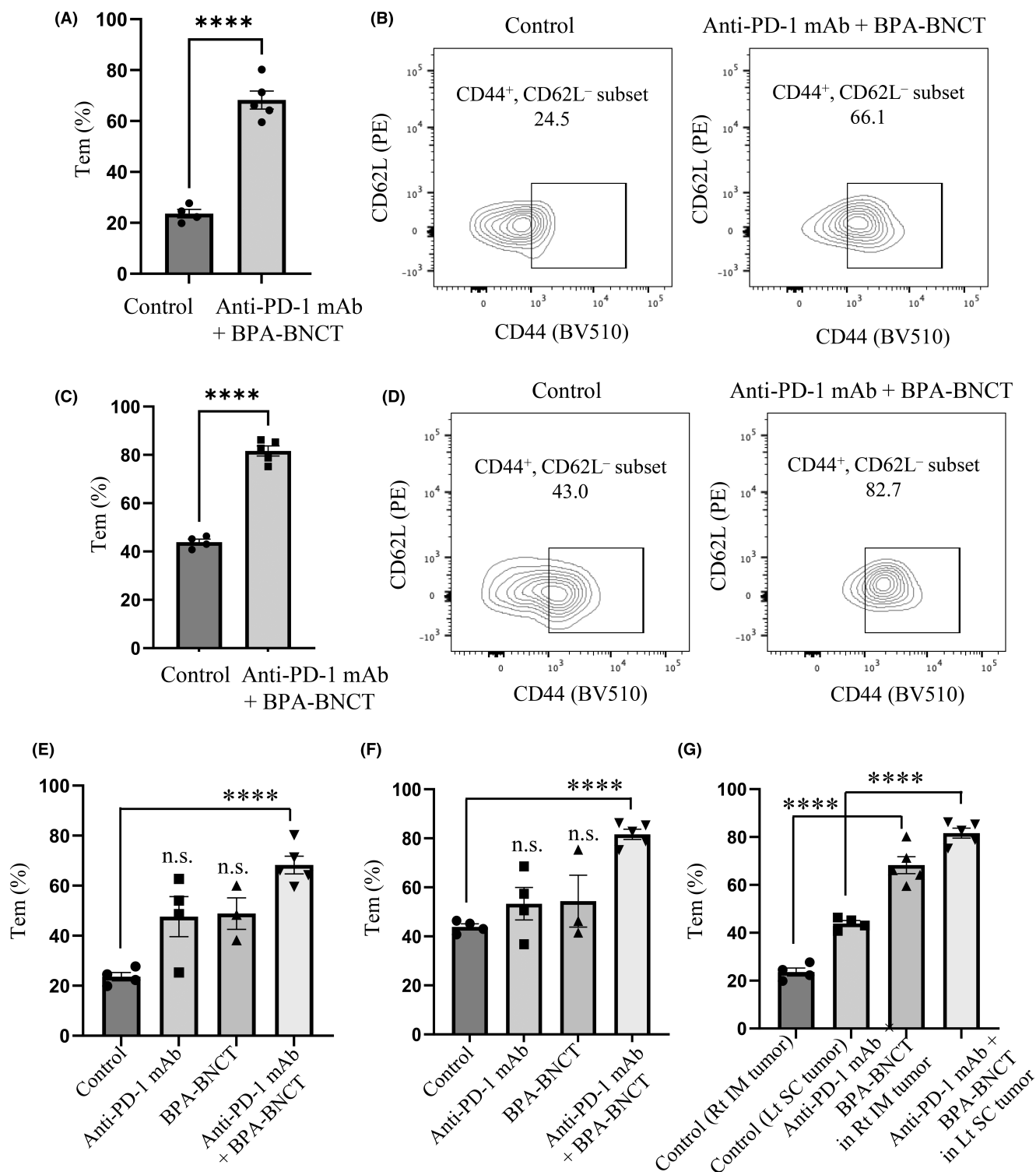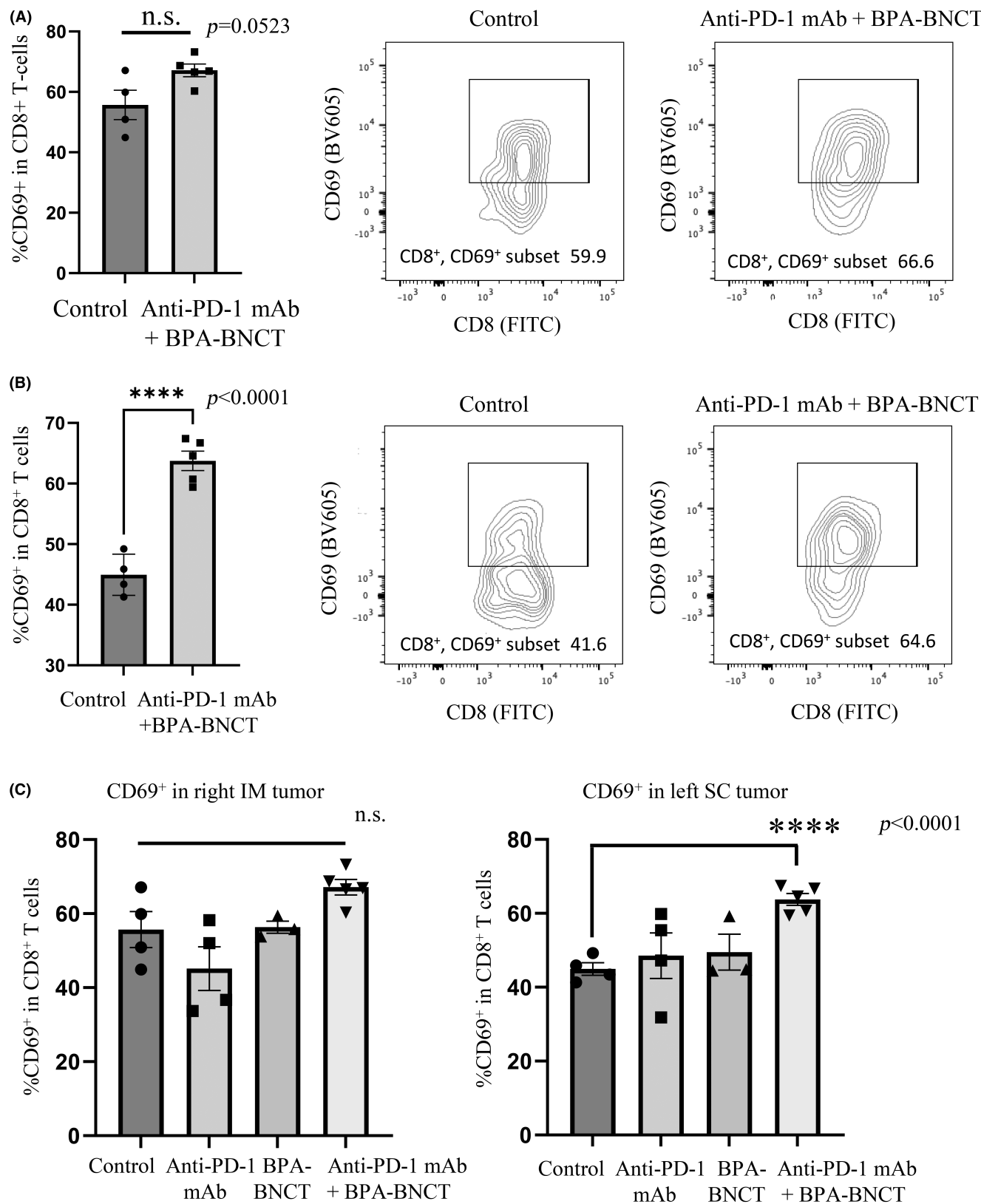
FIGURE 5 Analysis of tumor infiltrating lymphocytes of effector memory T cells (TEMs). (A–D) Flow cytometry analysis of effector memory T cells (CD44$^+$ CD62L- CD8$^+$, TEMs) in the right-thigh intramuscular tumors (A, B) ($p < 0.0001$) and in the left-flank subcutaneous tumor areas (neutron-shielded area) (C, D) ($p < 0.0001$). (E, F) Flow cytometry analysis of TEMs of four groups in the right intramuscular tumor (E) and left-flank subcutaneous tumor (F) ($p < 0.0001$). (G) Comparison of TEM results for both tumors between the control and B-NIT group ($p < 0.0001$). B-NIT, boron neutron immunotherapy; BNCT, boron neutron capture therapy; BPA, 4-borono-L-phenylalanine.

and to be applied to many advanced cancers that are ICI resistant. (Figure 9B). From the perspective of BNCT, it has been indicated for locally advanced or locally recurrent malignancies, but B-NIT

can facilitate BNCT for advanced cancers with lesions outside the neutron irradiation field. From an immunotherapy perspective, the contribution of combination therapy to improving response rates is

FIGURE 6 Analysis of tumor-infiltrating lymphocytes of early-activating T cells. (A, B) Flow cytometry analysis results of early-activating T cells ($CD8^+$ $CD69^+$) among the four groups. (A) Right-thigh intramuscular tumors, $p=0.0523$. (B) Left-flank subcutaneous tumor, $p<0.0001$ (C) Comparison of early-activating T cell results for both tumors between the control and B-NIT group ($p<0.0001$). B-NIT, boron neutron immunotherapy; BNCT, boron neutron capture therapy; BPA, 4-borono-L-phenylalanine.
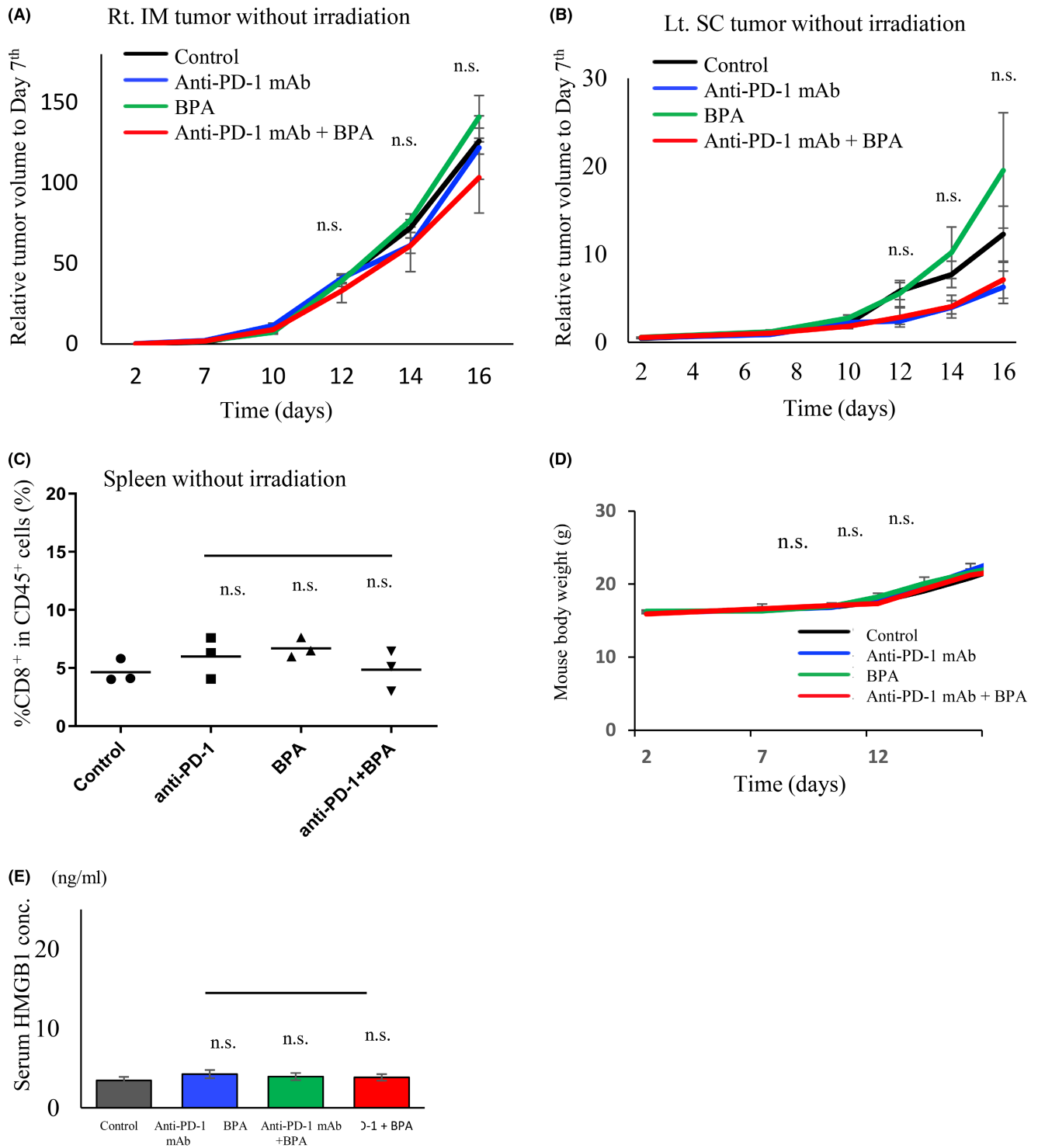
FIGURE 7 Results of treatment effects without neutron irradiation in four groups. (A, B) Tumor volume ratio results in four groups (control group, anti-PD-1 mAb group, BPA group, and anti-PD-1 mAb + BPA group) without neutron irradiation (right intramuscular tumor (A) and left lateral abdominal tumor (B), $n = 4$ per group). (C) Flow cytometry analysis of CD8+ T cells in CD45+ cells in spleen on day 16 ($n = 3$ per group). (D) Mouse body weight changes in the four groups over time ($n = 4$ per group). (E) Serum HMGB1 concentration (ng/mL) on day 16. BPA, 4-borono-L-phenylalanine.

FIGURE 8 Therapeutic effects of boron neutron immunotherapy (B-NIT) with anti-CD8-depleting mAb administration. (A) Schematic of B-NIT experiments with anti-CD8-depleting mAb ($n = 6$ per group). (B, C) Tumor volume ratio results at the right neutron irradiation site (B) and at the left shielded site (C) in six groups of four anti-CD8-depleting mAb groups (control, anti-PD-1 mAb, BPA-BNCT, B-NIT) and the two no-anti-CD8 mAb groups (control, B-NIT). (D) Tumor volume graph of the right tumor at the neutron-irradiation site (**$p < 0.01$) (E) Tumor volume graph of the left tumor at the shielded site (**$p < 0.01$). (F) Flow cytometry analysis of CD8+ CD45+ cells in spleen on day 16 ($n = 4$ per group). (G) Serum HMGB1 concentration (ng/mL) on day 16. (H) Mouse body weight (g) changes over time ($n = 6$) ($p = 0.125$).
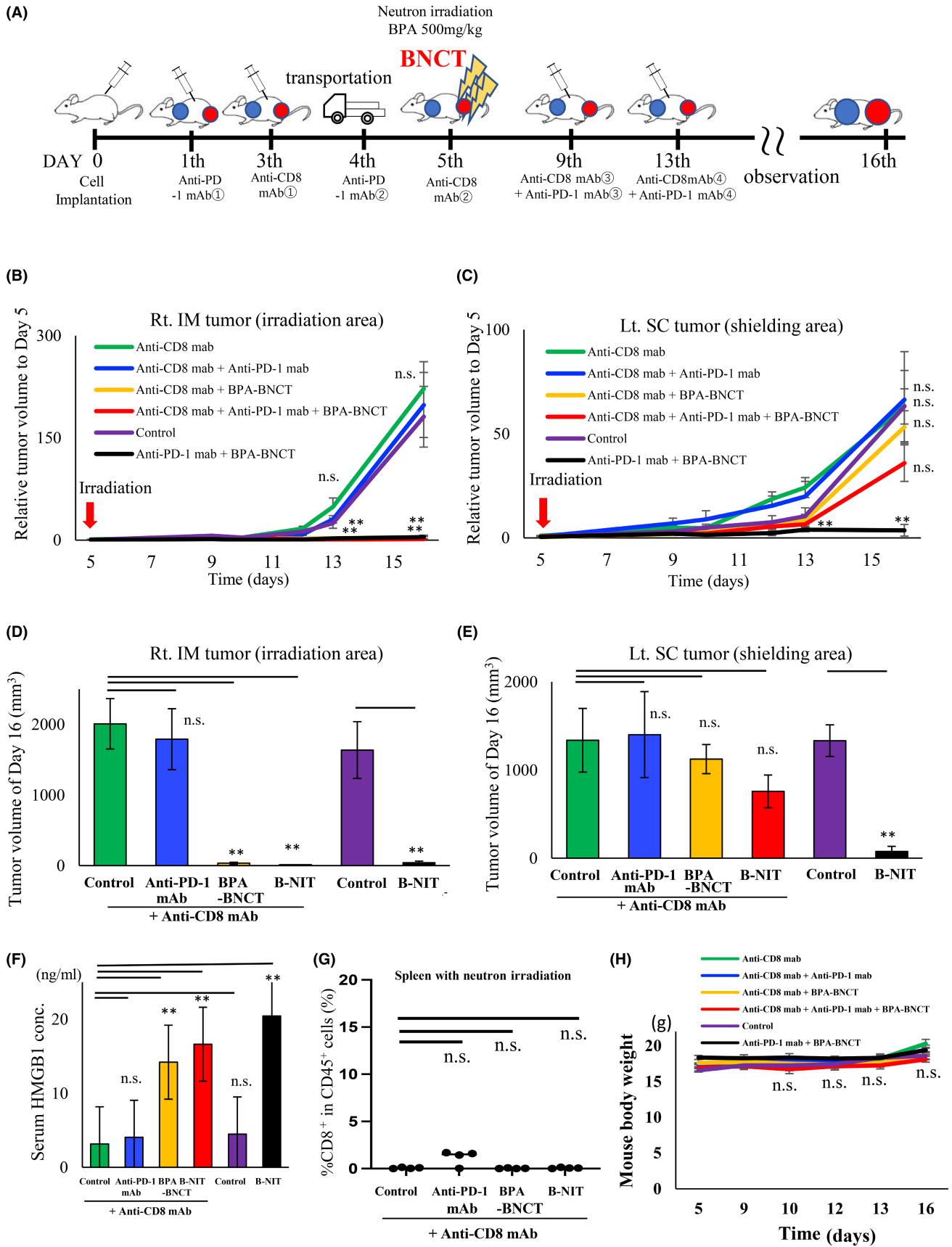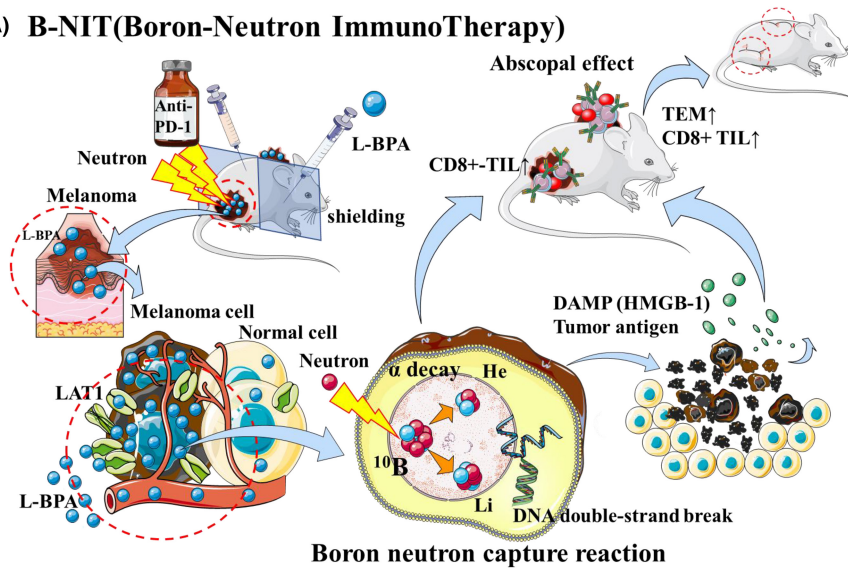
FIGURE 9 Graphic abstract of boron neutron immunotherapy (B-NIT). (A) Graphic abstract of B-NIT.(B) Image of B-NIT's future clinical direction.
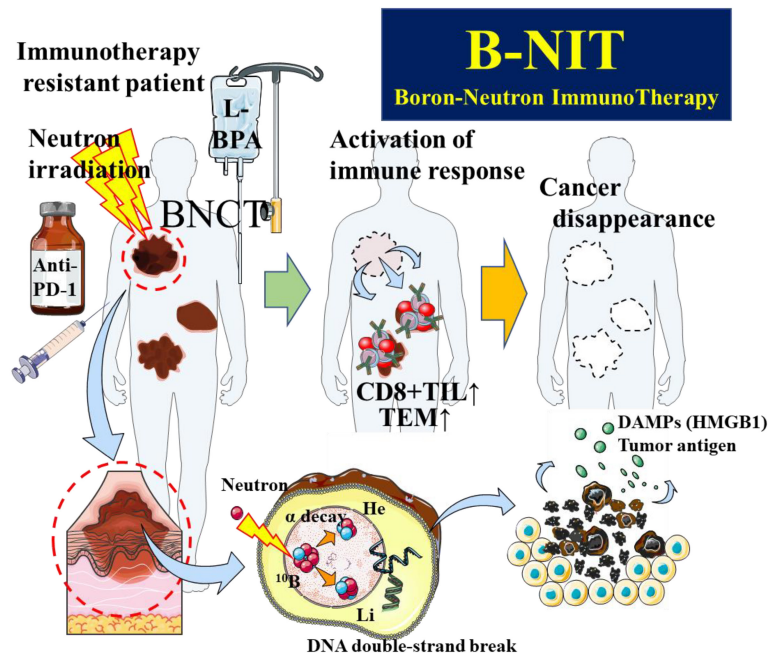
a very important finding for increasing the number of cured patients and expanding indications in the future.

Since the advent of ICIs, there have been a sharp increase in the number of case reports of abscopal effects with radiotherapy and ICI.[21-23] Radiation therapy induces DNA damage in tumors, activates stimulator of interferon gene (STING)-dependent pathways, increases tumor antigen expression, and induces activation of dendritic cells and T cells through the release of DAMPs, with effects on distant areas.[24] There are various options for the induction of the abscopal effect by radiotherapy, including the dose, number of irradiation fractions, beam source, and timing of treatment, and further optimization through future clinical trials is expected.[25-27] In a previous study, there was no significant difference in PFS or OS in advanced mucosal melanoma patients treated with ICI with or without radiotherapy.[28,29] Radiotherapy may also reduce antitumor immune responses by activating Langerhans cells and inducing regulatory T cells, and radiotherapy in cancer treatment should be carefully considered.[30] Next, the advantages and disadvantages of B-NIT compared with ICI plus radiotherapy are presented. The advantages of B-NIT are that BNCT reduces the dose to normal skin and increases the tumor dose, so the tumor microenvironment at the irradiated site is less affected; the treatment is completed with a single BNCT; and the immunotherapy schedule is not affected. The disadvantage is that facilities with neutron sources are available only in limited regions, such as Japan, limiting the number of facilities that can perform BNCT. Therefore, there is no evidence from clinical trials on B-NIT, and future clinical results are needed.

In this study, we observed an increase in splenic T lymphocytes after BNCT (Figure 4E), and an increase in TILs was confirmed at both the neutron irradiation site and distant site (Figures 4C,D). A high rate of TEMs and early-activating T cells with active antitumor effects were also confirmed at distant sites (Figure 4). Elevations of both TEMs and early-activating T cells in distant-site tumors suggested that B-NIT induced an abscopal effect.

We also confirmed high blood levels of HMGB1, which is a typical DAMP, following BNCT (Figures 2D,E). This indicates that the success of anticancer therapy and radiotherapy depends on innate and adaptive immune responses.[31] The strong cell-killing effect of BNCT-induced DNA double-strand breaks is assumed to contribute significantly to the induction of DAMPs.[26,32] The potent immune-inducing effect of all these B-NITs was evidenced by the results showing complete tumor growth inhibition (especially the abscopal effect at the shielding site) in 100% (6 out of 6 mice) of the B-NIT group observed in this study (Figure S8). However, under the administration of anti-CD8$^+$ depleting antibody, serum HMGB1 was elevated from the direct therapeutic effect of BNCT, but there was no therapeutic effect on the distant site (Figure 8).

Importantly, the demonstration of an abscopal effect with BNCT has established a new frontier in cancer treatment: combination therapy with ICI.[26,27] The oncolytic viral immunotherapy talimogene laherparepvec (T-VEC) was approved in the United States in 2015 for local treatment of patients with recurrent postoperative melanoma, and the safety of T-VEC in combination with ICIs (ipilimumab and pembrolizumab) was reported.[28,29] At our institution, Okayama University, the abscopal effect of another type of oncolytic virus used in preclinical trials in combination with ICI has been studied in a gastrointestinal surgery group.[33] Tavokinogene telseplasmid (TAVO) therapy, the direct injection of a plasmid encoding IL-12 into a tumor, in combination with pembrolizumab is a novel therapy for patients with advanced melanoma.[34]

Previously, the synergistic effects of combination treatment with immunotherapy and BNCT were reported.[35,36] These papers showed that the immunotherapeutic enhancing effects of BPA-BNCT in combination with Bacillus Calmette–Guerin (BCG) administration were also demonstrated in a colorectal cancer model. However, what cellular immunity is at work, which tumor immune mechanisms are activated, and what immunotherapy combination is best remained to be addressed.[35,36] This is the first paper to demonstrate the abscopal effect induced by the combination of BNCT and ICI in an ICI-resistant melanoma model. It is also the first paper to demonstrate CD8-mediated acquired immunity by BNCT. These results on B-NIT support the development of BNCT in new combination therapies for many malignancies that do not respond to ICI and will revolutionize cancer treatment.

AUTHOR CONTRIBUTIONS

Takuya Fujimoto: Formal analysis; investigation; resources; visualization; writing – original draft. **Osamu Yamasaki:** Funding acquisition; methodology; supervision. **Noriyuki Kanehira:** Investigation; resources; software. **Hirokazu Matsushita:** Investigation; methodology; resources; writing – original draft. **Yoshinori Sakurai:** Formal analysis; methodology; software; writing – original draft. **Naoya Kenmotsu:** Investigation; resources. **Ryo Mizuta:** Investigation; resources. **Natsuko Kondo:** Investigation; resources. **Takushi Takata:** Investigation; resources. **Mizuki Kitamatsu:** Investigation; resources. **Kazuyo Igawa:** Investigation; resources. **Atsushi Fujimura:** Investigation; resources. **Yoshihiro Otani:** Investigation; resources. **Makoto Shirakawa:** Supervision. **Kunitoshi Shigeyasu:** Supervision. **Fuminori Teraishi:** Funding acquisition; methodology; supervision. **Yosuke Togashi:** Project administration; supervision; writing – original draft. **Minoru Suzuki:** Supervision. **Toshiyoshi Fujiwara:** Project administration; supervision; writing – original draft. **Hiroyuki Michiue:** Conceptualization; funding acquisition; methodology; project administration; visualization; writing – original draft; writing – review and editing.

CONFLICT OF INTEREST STATEMENT

Japanese patent applications 2021-193305 and 2022-059950 "Drugs for the Treatment of Malignant Tumors" were applied by HM with the data in this paper. HM received collaborative research agreements and a research grant from Stella Pharma Corporation. YT received honoraria from Ono Pharmaceutical, Bristol-Myers Squibb, AstraZeneca, Chugai Pharmaceutical, and MSD and research grants from Ono Pharmaceutical, Bristol-Myers Squibb, AstraZeneca, Janssen Pharmaceutical K.K., Chugai Pharmaceutical, Daiichi-Sankyo, KOTAI biotechnologies, and KORTUC outside of this study. The other authors declare that they have no competing interests. Dr. Hirokazu Matsushita and Dr. Yosuke Togashi are editorial board members of *Cancer Science*.

DATA AVAILABILITY STATEMENT

The article includes all data in the study, and further inquiries can be directed to the corresponding author.

ETHICS STATEMENTS

Approval of the research protocol by an Institutional Review Board: N/A.
Informed Consent: N/A.
Registry and the Registration No. of the study/trial: N/A.
Animal Studies: All animal use and care procedures were conducted in accordance with the ARRIVE 2.0 guidelines and approved by

ORCID

Natsuko Kondo https://orcid.org/0000-0003-0895-4581
Atsushi Fujimura https://orcid.org/0000-0002-8638-5460
Yosuke Togashi https://orcid.org/0000-0001-9910-0164
Toshiyoshi Fujiwara https://orcid.org/0000-0002-5377-6051
Hiroyuki Michiue https://orcid.org/0000-0002-9215-4888

REFERENCES

1. Ishida Y, Agata Y, Shibahara K, Honjo T. A novel member of the immunoglobulin gene superfamily, upon programmed cell-death. *EMBO J*. 1992;11:3887-3895.
2. Iwai Y, Ishida M, Tanaka Y, Okazaki T, Honjo T, Minato N. Involvement of PD-L1 on tumor cells in the escape from host immune system and tumor immunotherapy by PD-L1 blockade. *Proc Natl Acad Sci USA*. 2002;99:12293-12297.
3. Leach DR, Krummel MF, Allison JP. Enhancement of antitumor immunity by CTLA-4 blockade. *Science*. 1996;271:1734-1736.
4. Carlino MS, Larkin J, Long GV. Immune checkpoint inhibitors in melanoma. *Lancet*. 2021;398:1002-1014.
5. Wolchok JD, Chiarion-Sileni V, Gonzalez R, et al. Overall survival with combined nivolumab and ipilimumab in advanced melanoma. *N Engl J Med*. 2017;377:1345-1356.
6. Wolchok JD, Chiarion-Sileni V, Gonzalez R, et al. Long-term outcomes with nivolumab plus ipilimumab or nivolumab alone versus ipilimumab in patients with advanced melanoma. *J Clin Oncol*. 2022;40:127-137.
7. Willsmore ZN, Coumbe BGT, Crescioli S, et al. Combined anti-PD-1 and anti-CTLA-4 checkpoint blockade: treatment of melanoma and immune mechanisms of action. *Eur J Immunol*. 2021;51:544-556.
8. Meric-Bernstam F, Larkin J, Tabernero J, Bonini C. Enhancing anti-tumour efficacy with immunotherapy combinations. *Lancet*. 2021;397:1010-1022.
9. Uhara H, Kiyohara Y, Uehara J, et al. Five-year survival with nivolumab in previously untreated Japanese patients with advanced or recurrent malignant melanoma. *J Dermatol*. 2021;48:592-599.
10. Jin WH, Seldon C, Butkus M, Sauerwein W, Giap HB. A review of boron neutron capture therapy: its history and current challenges. *Int J Part Ther*. 2022;9:71-82.
11. Nedunchezhian K, Aswath N, Thiruppathy M, Thirugnanamurthy S. Boron neutron capture therapy—a literature review. *J Clin Diagn Res*. 2016;10:1-4.
12. Mishima Y, Honda C, Ichihashi M, et al. Treatment of malignant melanoma by single thermal neutron capture therapy with melanoma-seeking 10B-compound. *Lancet*. 1989;2:388-389.
13. Wongthai P, Hagiwara K, Miyoshi Y, et al. Boronophenylalanine, a boron delivery agent for boron neutron capture therapy, is transported by ATB0,+, LAT1 and LAT2. *Cancer Sci*. 2015;106:279-286.
14. Hirose K, Konno A, Hiratsuka J, et al. Boron neutron capture therapy using cyclotron-based epithermal neutron source and borofalan ((10)B) for recurrent or locally advanced head and neck cancer (JHN002): an open-label phase II trial. *Radiother Oncol*. 2021;155:182-187.
15. Michiue H, Kitamatsu M, Fukunaga A, et al. Self-assembling A6K peptide nanotubes as a mercaptoundecahydrododecaborate (BSH) delivery system for boron neutron capture therapy (BNCT). *J Control Release*. 2021;330:788-796.
16. Iguchi Y, Michiue H, Kitamatsu M, et al. Tumor-specific delivery of BSH-3R for boron neutron capture therapy and positron emission tomography imaging in a mouse brain tumor model. *Biomaterials*. 2015;56:10-17.
17. Michiue H, Sakurai Y, Kondo N, et al. The acceleration of boron neutron capture therapy using multi-linked mercaptoundecahydro-dodecaborate (BSH) fused cell-penetrating peptide. *Biomaterials*. 2014;35:3396-3405.
18. Yamada S, Kitai Y, Tadokoro T, et al. Identification of RPL15 60S ribosomal protein as a novel topotecan target protein that correlates with DAMP secretion and antitumor immune activation. *J Immunol*. 2022;209:171-179.
19. Zhu Z, Tang R, Huff S, et al. Small-molecule PTPN2 inhibitors sensitize resistant melanoma to anti-PD-1 immunotherapy. *Cancer Res Commun*. 2023;3:119-129.
20. Curti BD, Faries MB. Recent advances in the treatment of melanoma. *N Engl J Med*. 2021;384:2229-2240.
21. Hiniker SM, Chen DS, Knox SJ. Abscopal effect in a patient with melanoma. *N Engl J Med*. 2012;366:2035-2036.
22. Postow MA, Callahan MK, Barker CA, et al. Immunologic correlates of the abscopal effect in a patient with melanoma. *N Engl J Med*. 2012;366:925-931.
23. Formenti SC, Rudqvist NP, Golden E, et al. Radiotherapy induces responses of lung cancer to CTLA-4 blockade. *Nat Med*. 2018;24:1845-1851.
24. Chang MC, Chen YL, Lin HW, et al. Irradiation enhances abscopal anti-tumor effects of antigen-specific immunotherapy through regulating tumor microenvironment. *Mol Ther*. 2018;26:404-419.
25. Umeda Y, Yoshikawa S, Kiniwa Y, et al. Real-world efficacy of anti-PD-1 antibody or combined anti-PD-1 plus anti-CTLA-4 antibodies, with or without radiotherapy, in advanced mucosal melanoma patients: a retrospective, multicenter study. *Eur J Cancer*. 2021;157:361-372.
26. Rohatgi A, Kirkwood JM. Beyond PD-1: the next frontier for immunotherapy in melanoma. *Front Oncol*. 2021;11:640314.
27. Vafaei S, Zekiy AO, Khanamir RA, et al. Combination therapy with immune checkpoint inhibitors (ICIs); a new frontier. *Cancer Cell Int*. 2022;22:2.
28. Dummer R, Gyorki DE, Hyngstrom J, et al. Neoadjuvant talimogene laherparepvec plus surgery versus surgery alone for resectable stage IIIB-IVM1a melanoma: a randomized, open-label, phase 2 trial. *Nat Med*. 2021;27:1789-1796.
29. Chesney J, Puzanov I, Collichio F, et al. Patterns of response with talimogene laherparepvec in combination with ipilimumab or ipilimumab alone in metastatic unresectable melanoma. *Br J Cancer*. 2019;121:417-420.
30. Price JG, Idoyaga J, Salmon H, et al. CDKN1A regulates Langerhans cell survival and promotes Treg cell generation upon exposure to ionizing irradiation. *Nat Immunol*. 2015;16:1060-1068.
31. Apetoh L, Ghiringhelli F, Tesniere A, et al. Toll-like receptor 4-dependent contribution of the immune system to anticancer chemotherapy and radiotherapy. *Nat Med*. 2007;13:1050-1059.
32. Kondo N, Michiue H, Sakurai Y, et al. Detection of gammaH2AX foci in mouse normal brain and brain tumor after boron neutron capture therapy. *Rep Pract Oncol Radiother*. 2016;21:108-112.
33. Kanaya N, Kuroda S, Kakiuchi Y, et al. Immune modulation by telomerase-specific oncolytic adenovirus synergistically enhances antitumor efficacy with anti-PD1 antibody. *Mol Ther*. 2020;28:794-804.
34. Dollin Y, Rubin J, Carvajal RD, Rached H, Nitzkorski JR. Pembrolizumab and tavokinogene telseplasmid electroporation in metastatic melanoma. *Int J Surg Case Rep*. 2020;77:591-594.
35. Trivillin VA, Pozzi ECC, Colombo LL, et al. Abscopal effect of boron neutron capture therapy (BNCT): proof of principle in

an experimental model of colon cancer. *Radiat Environ Biophys.* 2017;56:365-375.

36. Trivillin VA, Langle YV, Palmieri MA, et al. Evaluation of local, regional and abscopal effects of boron neutron capture therapy (BNCT) combined with immunotherapy in an ectopic colon cancer model. *Br J Radiol.* 2021;94:20210593.

SUPPORTING INFORMATION

Additional supporting information can be found online in the Supporting Information section at the end of this article.